Phenomenology of tremor-like signals observed over hydrocarbon reservoirs

S. Dangel [a,*], M.E. Schaepman [a], E.P. Stoll [a], R. Carniel [b], O. Barzandji [c],
E.-D. Rode [c], J.M. Singer [c]

[a] Remote Sensing Laboratories, Universität Zürich, Winterthurerstrasse 190, CH-8057 Zürich, Switzerland
[b] Dipartimento di Georisorse e Territorio, Universitá di Udine, Via Cotonificio, 114, 33100 Udine, Italy
[c] ADNR Technology Services Sagl, Via San Gottardo 56, CH-6648 Minusio, Switzerland

Abstract

We have observed narrow-band, low-frequency (1.5–4 Hz, amplitude 0.01–10 µm/s) tremor signals on the surface over hydrocarbon reservoirs (oil, gas and water multiphase fluid systems in porous media) at currently 15 sites worldwide. These 'hydrocarbon tremors' possess remarkably similar spectral and signal structure characteristics, pointing to a common source mechanism, even though the depth (some hundreds to several thousands of meters), specific fluid content (oil, gas, gas condensate of different compositions and combinations) and reservoir rock type (such as sandstone, carbonates, etc.) for each of those sites are quite different. About half of the sites are fully explored or even developed and producing fields, and hard quantitative data on the reservoirs are available (well data, reservoir monitoring data, seismic surveys, etc.). The other areas are essentially either explored prospect areas where we did not have access to hard reservoir data or (in only one case) areas where no exploration wells have been drilled at all. The tremor signal itself was observed over ALL locations investigated so far. The signals weaken at the rim of the reservoirs and are not observed outside the reservoir area. There is a strong correlation of the tremor power with the thickness of the hydrocarbon-bearing layers ('pay zone thickness') determined by borehole log measurements. The overall correlation between surface tremor measurements and accessible subsurface well data is higher than 90%. The phenomenological comparison of hydrocarbon tremor signals with volcanic tremor signals from Stromboli and Arenal volcanoes using both conventional spectral analysis tools and non-linear dynamics methods reveals fundamental similarities between those two phenomena as well as their close relation to bandpass filtered noise. Nevertheless, the specific signal sources are expected to be different for volcanoes and hydrocarbon reservoirs. Using the currently available data we present possible concepts (active or passive mechanisms) on the nature of the hydrocarbon tremor source. Our data lead us to conclude that we are most likely observing a characteristic filtering/ mixing effect, with the energy input supplied by the natural seismo-acoustic background. The reservoir, i.e. the hydrocarbon-water-multifluid system contained in a porous medium, is expected to be the oscillatory element able to act as a filter/mixer (resembling essentially a in-reservoir path effect) for the natural seismo-acoustic background. Most intriguing seems the application aspect, i.e. the practical usability of this spectroscopic approach as a direct from-the-surface, non-invasive hydrocarbon indicator.
© 2003 Elsevier B.V. All rights reserved.

* Corresponding author. Tel.: +41-1-635-6817; Fax: +41-1-635-6846.
  E-mail addresses: dangel@geo.unizh.ch (S. Dangel), carniel@dgt.uniud.it (R. Carniel), johannes.singer@gmx.ch (J.M. Singer).

1. Introduction

We apply a seismic spectroscopy method relying on seismometers (highly sensitive ground motion velocity receivers) placed on the surface over hydrocarbon reservoirs. Using such a spectroscopic approach we discovered a new kind of tremor-like signal, later on dubbed 'hydrocarbon tremor' (Dangel and Singer, 2002).

There exist numerous continuous seismic signals which are usually rather weak and which were (and sometimes still are) often considered as useless ('seismo-acoustic') background noise only. However, this 'noise' can carry useful information which is contained in its characteristics, such as the frequency spectrum, statistical properties or non-linear behavior. Moreover, it may contain a spectral signature characteristic of the media or environment which it has passed through. A certain broadband seismo-acoustic background noise is present at every location around the world. Examples of characteristic signatures found in the background noise include the movement of the earth's crust due to standing ocean waves (Aki and Richards, 1980) with spectral peaks in the 0.1–0.2 Hz range, or the observation of the eigenmodes of the terrestrial crust (Suda et al., 1998) with spectral peaks in the millihertz range. Another kind of continuous seismic signals can be observed near volcanoes and glaciers; it is termed 'tremor' in the literature (Ferrick et al., 1982; Ripepe and Gordeev, 1999; Wolf and Davies, 1986; Julian, 1994; Urquizú and Correig, 1999; Carniel and DiCecca, 1999). Tremor can be defined as a sustained seismic signal within a limited frequency range.

Describing the hydrocarbon tremor, we report the discovery of a structurally similar signal observed over hydrocarbon reservoirs (oil, gas and water multiphase fluid systems in porous media). It is characterized by peaks ('spectral lines') in the [1.5–4] Hz range, quasi-continuous duration and a correlation time of several seconds. Up to now we have confirmed this finding at 15 major hydrocarbon sites worldwide – areas including both currently producing and virgin reservoirs. In all cases, this characteristic tremor signal was absent (or its amplitude several orders of magnitude weaker) at the rim of or outside the reservoir areas (as verified at 'proven' non-hydrocarbon locations: 'dry holes'). Moreover, preliminary tests using a directionally sensitive sensor setup (a triangular array of triaxial sensors on the surface) showed that the signal components containing the tremor phenomenon originate from the direction of the reservoir. Thus, the phenomenon can be definitely attributed to the reservoir zone. However, the present paper is exclusively devoted to the observation and spectroscopic identification of the basic hydrocarbon tremor phenomenon. Forthcoming reports will focus on other aspects, including topics like polarization, direction and depth evaluation. Using a surface measurement alone, it is not possible to clearly distinguish between a signal actively emitted by the reservoir or a signal which has been characteristically deformed or filtered by the reservoir. In other words, our spectroscopic approach investigates a characteristic signal without distinguishing if it is either actively emitted by a source within the reservoir (real source) or being the result of a characteristic filtering of a seismo-acoustic background signal (in this picture the virtual spectroscopical 'light' source) passed through the reservoir.

At present, the microscopic source mechanism of this hydrocarbon reservoir tremor is still open to speculation. Although there seems to be an astonishing similarity in terms of signal type, properties and structure to volcanic tremor, the specific signal sources are naturally expected to be different for volcanoes and hydrocarbon reservoirs.

2. Experimental setup

The signals were recorded using two different

velocity sensors: an electrochemical design based on the commercially available Sprengnether WB-2023 with sensitivity 1500 V/m/s and natural period 20 s (comparable to well-known sensors like the Guralp CMG-3 ESP, with a 30-s natural period and sensitivity of 1500 V/m/s), and an ADNR proprietary electromechanical construction of the moving coil type with sensitivity 30 000 V/m/s and natural period 2 s. We are not aware of any commercial sensor with such a high sensitivity, neither in the short period nor in the broadband category. Typical 1-s or 2-s sensor sensitivities are well below 1000 V/m/s.

For field measurements the sensors are placed in covered holes at about 1 m depth for firm ground contact and wind shielding. The field setups are either synchronous measurements with a small sensor array (4–8 sensors recording concurrently) or asynchronous measurements, where larger areas are covered by placing a setup of 2–4 sensors at a particular location, recording for a period of time and then shifting the setup to the next location. For phase evaluations synchronous measurements are obviously the only way to go

(this, e.g. includes directional measurements or depth triangulation experiments). In contrast, for a purely amplitude-focused spectroscopy approach we regard both methods roughly equal as long as the asynchronous setups are recording sufficiently long stationary tremor signals. The advantage of the asynchronous measurement is of purely pragmatic nature, as we are not able to deploy enough sensors to cover long profiles or large arrays synchronously. Most of the 15 sites described in Section 3 have been investigated using both approaches; in the present paper we can only focus on the basic identification of the hydrocarbon tremor phenomenon. Possible field setups are 1-D ('profiles') or 2-D grids ('arrays'). The measurement duration is typically 40 min at 100-Hz sampling rate. This duration allows for the recording of sufficiently long signal windows such that unwanted transient noises (e.g. man-made noise like trucks passing nearby, etc.) can be removed, leading to clean and stationary signals which can be compared between different locations. Afterwards the signals are processed and evaluated according to typical seismic spectrosco-
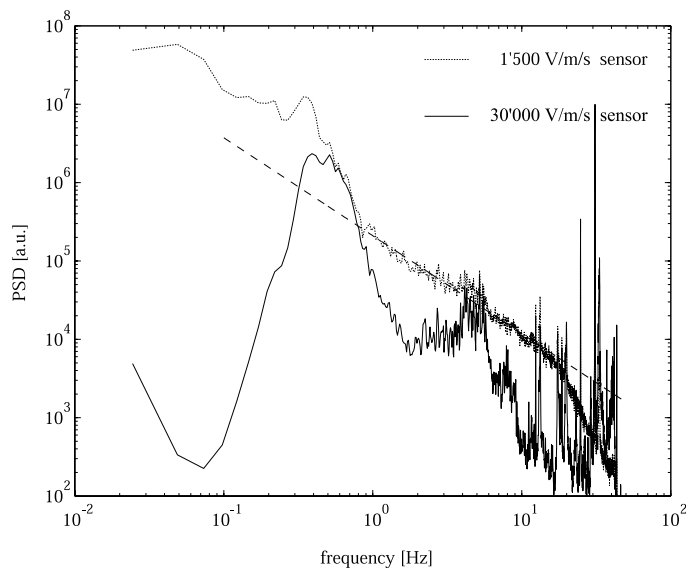

Fig. 1. Comparison of the two sensors, the electrochemical 1500 V/m/s and the electromechanical 30 000 V/m/s. The recording took place synchronously with both sensors placed right next to each other. The velocity data and spectra have been left unfiltered. The dashed line denotes the internal noise level of the 1500 V/m/s sensor, which seems to follow a perfect f^{-n} behavior over more than a decade. The power spectral density (PSD) is plotted in arbitrary measuring units (recorder counts) against frequency.
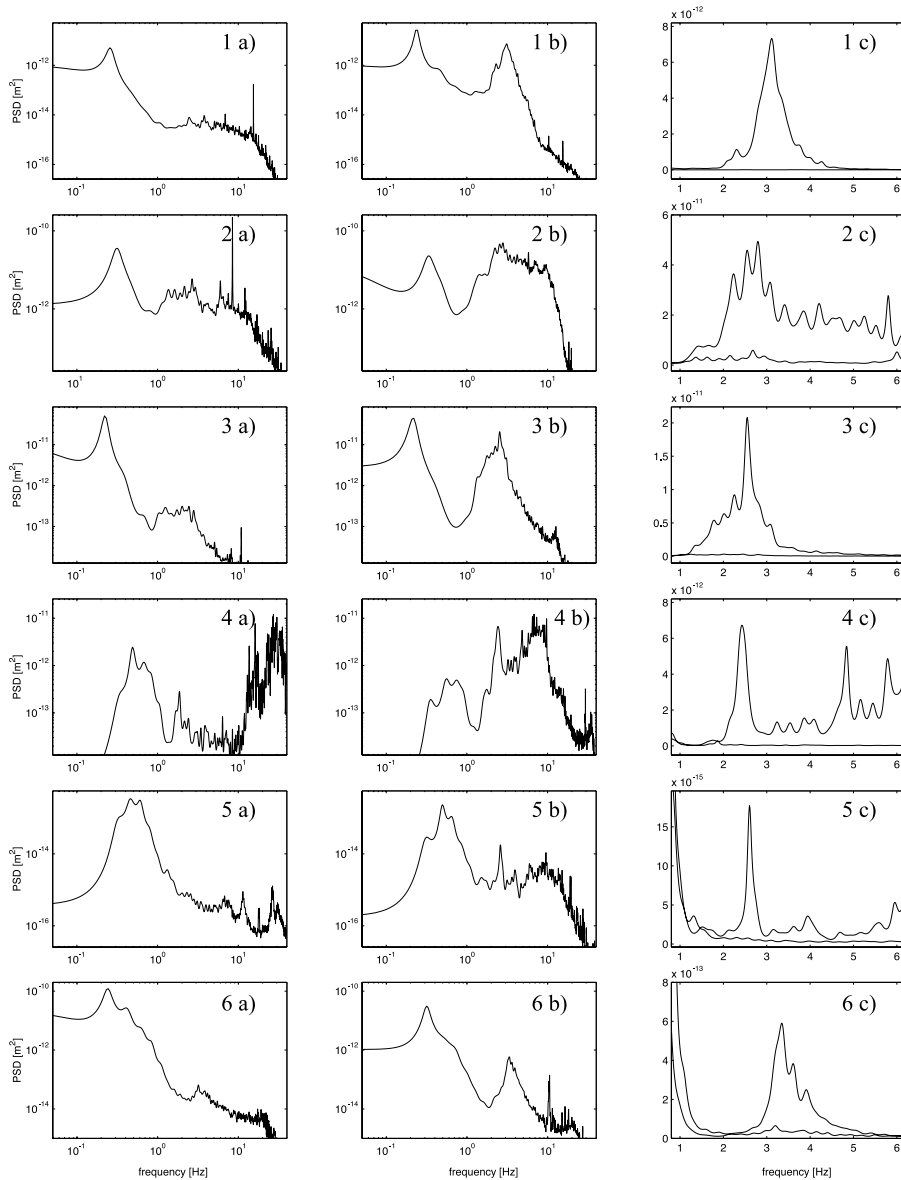
Fig. 2. Vertical velocity power spectra recorded on the surface over hydrocarbon reservoirs at different locations of Europe and the Middle East. Spectra labeled (a) correspond to proven non-hydrocarbon locations near a reservoir area; spectra labeled (b) correspond to proven hydrocarbon locations inside the same reservoir area. Spectra labeled (c), third column, show (a) and (b) combined as linear plot (to emphasize the enormous difference between the hydrocarbon and non-hydrocarbon signal in the narrow frequency window investigated for hydrocarbon presence, i.e. 1–6 Hz). In (c) the upper curve is always the hydrocarbon signal, whereas the lower one is the non-hydrocarbon. Note the different scales of the vertical axes. Key to sites: 1, Jordan, proven exploration prospect; 2, Italy, developed field; 3, Ukraine, developed field; 4, UAE, developed field; 5, UAE, proven exploration prospect; 6, Morocco, unproven oil prospect; 7, Italy 2, producing gas field (the narrow peak at approximately 1.4 Hz in the reservoir signal is attributed to a identified downhole pumping system); 8, Ukraine 2, producing gas field; 9, Switzerland, non-producing, but proven gas reservoir; 10, Switzerland 2, gas prospect; 11, Ukraine 3, producing gas reservoir; 12, UAE, Emirate of Dubai, undeveloped prospect.
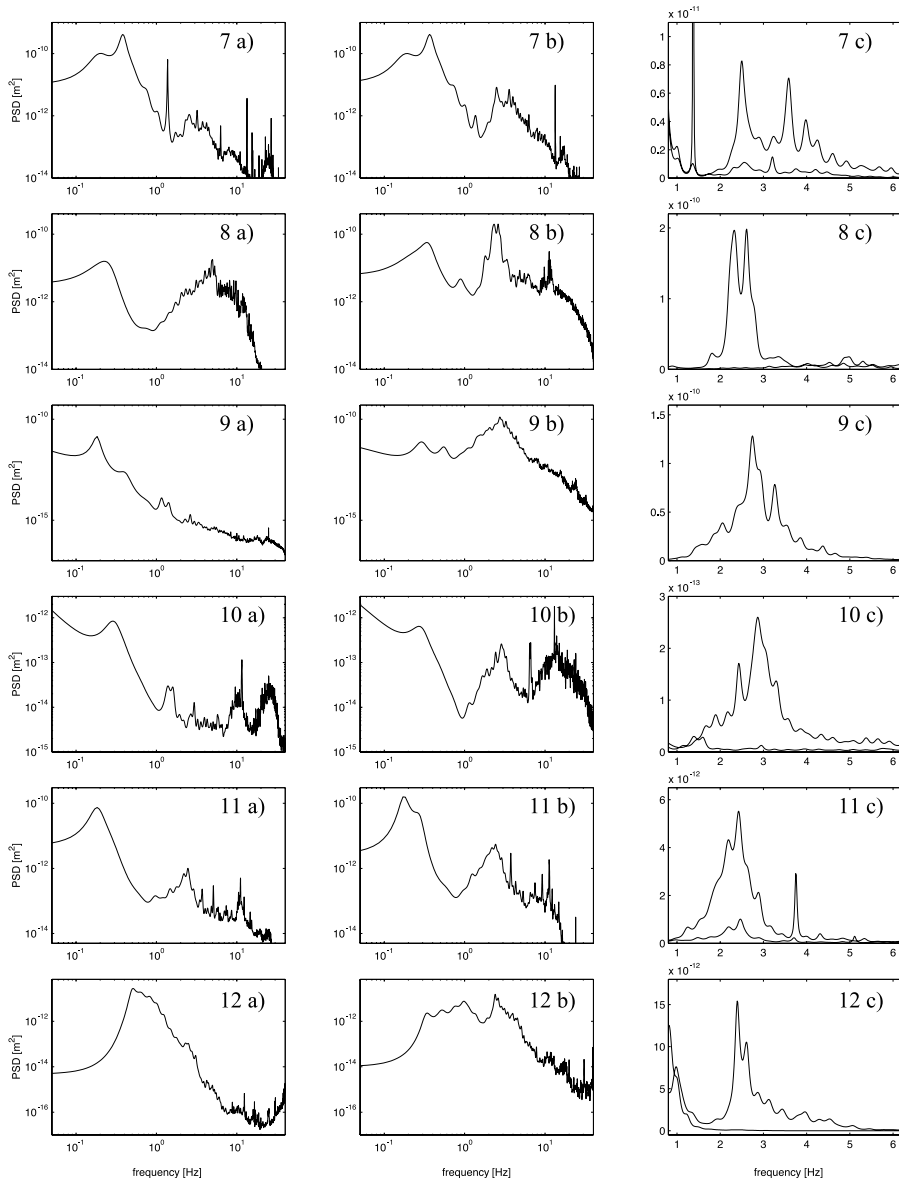
Fig. 2 (*Continued*).

py procedures, also applied e.g. to volcanic tremor (Urquizú and Correig, 1999; Carniel and Iacop, 1996).

The most important difference to conventional seismic spectral analysis is the overall signal amplitude level in the frequency window of interest. It is obviously much lower above a hydrocarbon reservoir than near a strong signal source such as a volcano. This is particularly true in known seismically/tectonically 'quiet' environments such as the central Arabian desert 'Empty Quarter' as found in the south of the United Arab Emirates (UAE; see site 5, below). The necessary prerequisite for the identification of hydrocarbon tremor in such a quiet area is indeed the availability of sensors with a sensitivity much better than the

available commercial sensors can provide. This is illustrated in Fig. 1, showing two spectra recorded synchronously with the 1500 V/m/s and the 30 000 V/m/s sensor at the very same spot. The difference is obvious, with the more sensitive sensor showing a distinct external signal where the less sensitive one reproduces only the characteristic internal 1/f equipment noise. Nevertheless, the basic phenomenon 'hydrocarbon tremor' is observable in more 'conventional' locations (conventional in terms of their seismo-acoustic background amplitude level) using commercial seismometers such as the Sprengnethers; the fundamental measurability of the hydrocarbon tremor does not depend on the ADNR proprietary design. Only in ultra quiet locations such as the above described 'Empty Quarter' the ADNR design is essential for the basic observation. The ADNR design has two additional advantages, namely the considerably lower internal electronic and mechanic noise level, giving rise to a spectroscopic interpretation requiring much less signal filtering steps, plus a construction feature (double coil signal pick up system) to eliminate any possible electromagnetic component in this frequency regime. Likewise, the commercially available Sprengnether is by its very design (electrochemical) insensitive to electromagnetic components. It should be noted, however, that a 'simple' geophone construction, as it is typically used in reflection seismic campaigns, is – due to its very design specifications (frequency- and amplitude-wise) – not suited for the presented spectroscopic approach.

3. Phenomenology

3.1. Description of sample hydrocarbon tremor sites

Fig. 2 shows a series of examples of spectra observed over hydrocarbon reservoirs situated at several different locations around Europe and the Middle East. Vertical velocity time series from single seismometers located at hydrocarbon-bearing wells (b) as well as at known non-hydrocarbon locations (a), both within the same reservoir area, have been used. After selecting artifact-free

(this refers mostly to surface transients) windows of about 600 s duration, power spectra were calculated using the maximum entropy method (Press et al., 1992) with 400 poles. With the exception of site 6, all reservoir and non-reservoir locations are proven by exploration holes. Sites 4, 5 and 12 have been recorded using the electromechanical 30 000 V/m/s sensor, all other sites using the electrochemical 1500 V/m/s sensor. (Site 5 was recorded twice with a time lapse of 5 month in between with both, electrochemical and ADNR electromechanical sensors.)

● Site 1 is an oil prospect in Jordan within the Dead Sea Rift Valley which was not developed at the time of the measurements in May 2000. Old and abandoned exploration wells were identified. Drilling of a new exploration well and the confirmation of the hydrocarbon reservoir took place roughly one year later. The depth of the reservoir is between 2 and 4 km, the reservoir rocks are clastics. The distance between recording points (a) and (b) is 4.5 km.

● Site 2 is a developed and producing oil field in northern Italy close to the industrial belt of Milan. The depth of the oil horizon is approximately 5 km, the distance between the recording points (a) and (b) is about 1.5 km.

● Site 3 is a gas reservoir (partially producing, partially in development) in central Ukraine. The depth of the reservoir is approximately 3 km, the reservoir rocks are clastics, and the distance between the two shown measuring points is about 2 km.

● Site 4 is a heavily developed and producing oil reservoir located in the Emirate of Abu Dhabi, UAE. The reservoir is exploited via the water injection technique at the periphery of the reservoir. The reservoir rocks are carbonates, the depth of the oil horizon is approximately 2.5 km, and the distance between the two recording points is 4.5 km.

● Site 5 is a confirmed (via exploration wells), but not yet developed or producing reservoir in the Emirate of Abu Dhabi, UAE. The reservoir system is comprised of carbonate rocks. The depth of the reservoir is approximately 2.1 km, the distance between the recording points is 5.6 km.

● Site 6 is an oil prospect in Morocco. The rock type is carbonates, the depth 1.5–2 km and the distance between the two points 5 km.

● Site 7 is a proven and producing gas field in central Italy, distance 0.6 km, depth 0.8 km, rock type Clastics. The narrow peak at about 1.4 Hz is a man-made artifact originating from a pump.

● Site 8 is another proven and producing gas field in Ukraine (different from site 3), distance 4.5 km, depth 4 km, rock type Clastics.

● Site 9 is a non-producing, but proven gas reservoir in southern Switzerland, distance 12 km, depth less than 1 km, rock type Clastics.

● Site 10 is a gas prospect in northern Switzerland, distance 2 km, depth less than 1 km, rock type Clastics.

● Site 11 is yet another proven and producing gas reservoir in Ukraine (again different from both of the previously mentioned sites 3 and 8), distance 2.4 km, depth 4–4.5 km, rock type Clastics. Point (b) is at the rim of the reservoir; we have no data totally outside the proven reservoir area.

● Site 12 is an undeveloped prospect in the Emirate of Dubai, UAE. Old abandoned exploration wells show extensive gas content. The reservoir is of the carbonate type, Thamama group, and deeper than 3.5 km.

In addition to the 12 sites presented in Fig. 2, we very recently recorded data at another series of sites. Those measurements are not yet fully processed and interpreted and, thus, not cleared for presentation in a scientific publication by the particular concession owners/operators. Nevertheless, the basic findings, i.e. the appearance of the hydrocarbon tremor as well as its correlation to reservoir properties (see discussion below), fit excellently into the picture derived from the previous dozen measurements, discussed above: sites 13–15. Site 13 is a gas/gas condensate producing developed field in the Emirate of Dubai, UAE, Oman thrust fault zone; it is actually a bipartite reservoir (one structure with a permeability barrier). Again, this reservoir is of the carbonate type, Shuaiba reservoir zone, approximately 2.5 km deep. Sites 14 and 15 are recordings from the USA, State of Texas, one being located in a dense chalk formation ('Austin Chalk' Forma-
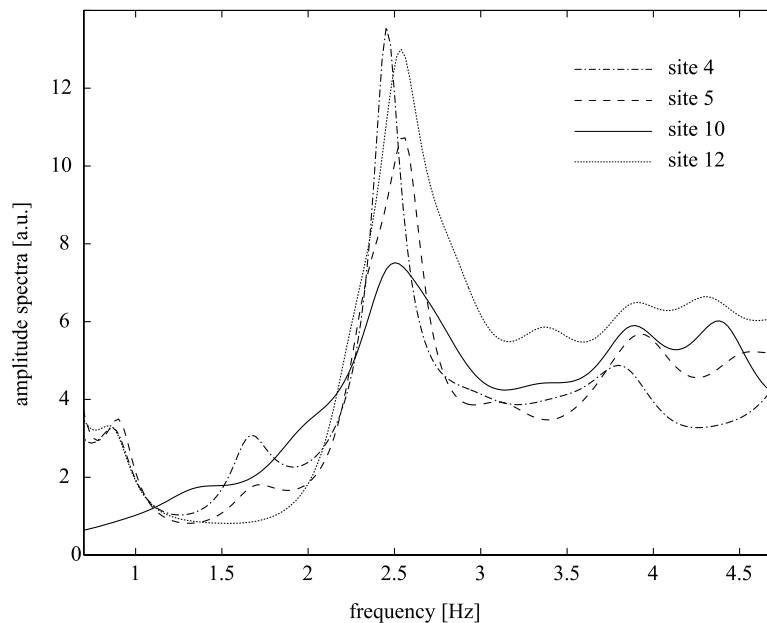

Fig. 3. Direct comparison of amplitude spectra of hydrocarbon locations of sites 4, 5, 10 and 12, not to scale. An arbitrary stretching factor in the amplitude as well as an arbitrary shift (up to 0.5 Hz) along the frequency axis were used to 'match' the signals visually. The purpose of this plot is to visualize the extreme structural similarity of signals obtained at completely different locations.

tion, Eastern Texas, porous system, but almost no permeability; production comes from fractures only, depth approx 2–3 km), whereas the other one is from a rather shallow (600–800 m) highly porous and highly permeable sand channel system (Upper Tannhill system, Central Texas).

Fig. 3 shows superimposed spectra (not to scale) corresponding to the hydrocarbon locations of sites 4, 5, 10, and 12 for direct comparison. The signals were rescaled to allow visual comparison of the overall similar spectroscopic 'fingerprint' caused by the hydrocarbon emplacements. Contemplating the collection of spectra of Figs. 2 and 3, we note the following facts:

● Even though the depth, fluid content, rock types and overlying geology of the reservoirs are quite different, all observed hydrocarbon tremor spectral peaks lie within a remarkably narrow frequency range of about 1.5–4 Hz. This speaks in favor of a source rather than a path effect.

● The mean absolute power of the hydrocarbon tremor depends on the level of the environmental noise (amplitude of the seismo-acoustic background). At one extreme we have site 5 which is situated in an absolutely quiet desert corner in the UAE and shows the weakest tremor signals (amplitude around 0.01 μm/s), on the other extreme are sites 8 and 9, both of which lie within industrial zones and exhibit the strongest hydrocarbon tremor signals up to this date (amplitudes around 10 μm/s). This implies that the environmental seismo-acoustic noise is a probable source of energy for the tremor signals. The noise would have to be partially converted or filtered by the reservoir system (multiphase fluid filled porous rocks), resulting in the tremor signals. This might speak in favor of a kind of path effect.

● The number of spectral peaks within the hydrocarbon tremor frequency band varies moderately. Some locations, such as the UAE fields, show sometimes several distinct peaks, typically about four, others are dominated by a single peak only. We speculate that the occurrence of a dominating main peak may be connected with the presence of salt domes (such as at site 12, Dubai coastal area) or thick surface salt pillows (such as site 1, Dead Sea).

● Other features visible in a broadband spectro-

scopic evaluation include the well-known oceanic microseism (visible at around 0.1 Hz, depending on the location and on the type of sensor used), local effects of sea waves (typically around 0.5–1 Hz), and man-made artifacts. The latter are typically characterized by higher frequency components, but sometimes there are artifacts such as the pump operating at approximately 1.4 Hz at site 7. These kind of artifacts can easily be identified and removed.[1]

3.2. Comparison to volcanic tremor and artificial data

In order to compare hydrocarbon tremor to volcanic tremor phenomenologically, we select a series of signals. Although the selection of sites and signals was done quite arbitrarily, the selection criterion applied is that we take signals of which the particular properties can be detected without any significant preprocessing/filtering, in order to avoid an introduction of possible artificial effects due to specific processing or treatment. Nevertheless, the demonstrated properties do in principle apply to all signals recorded at all sites. Moreover, we deliberately select recordings done with commercially available sensors (the Sprengnethers) to avoid 'black box effect' speculations about signals observable with proprietary sensors only.

From the results of the different data comparison methods, as discussed below, we arrive at the following conclusions.

● Both kinds of tremor signals, of hydrocarbon reservoir and volcanic origin, as well as an artificially constructed high dimensional signal, have very similar behavior when subjected to a broad variety of signal processing tools. We therefore conclude that the tremor signals can be characterized as narrow band noise. This has some implications on possible models explaining their origin, as discussed in Section 4.

● The sensitivity of some of these signal processing tools can be used to distinguish 'false'

---

[1] For a very illustrative discussion of the ambient seismo-acoustic background, we refer to web page: www.seismo.com.
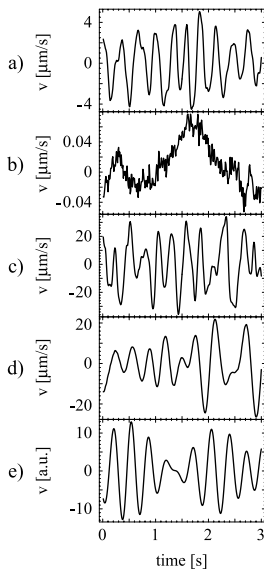
Fig. 4. Raw velocity data of hydrocarbon, volcanic and artificial tremor signals, 3 s time window. (a) Hydrocarbon location of site 9. (b) Non-hydrocarbon location of site 9 (note different scale). (c) Stromboli volcano. (d) Arenal volcano. (e) Artificial signal.

spectral peaks in the usual frequency range of 1.5–4 Hz (resulting from artificial noise)[2] from 'true' peaks resulting from hydrocarbon or volcanic tremor. For practical purposes, the most efficient true/false discrimination can be achieved by using the correlation filter (see below) and by comparing the structure functions of the first differences of the signals.

Signal selection:

• Signal (a) is the hydrocarbon location signal of site 9, as shown in Fig. 2, recorded using the electrochemical sensor at 100 Hz, length 1 h.

• Signal (b) is the non-hydrocarbon location signal of site 9, as shown in Fig. 2, recorded using the electrochemical sensor at 100 Hz, length 1 h.

---

[2] Here we denote 'noise' as either spectrally or timewise identifiable signal contributions coming typically from the ambient surface ('artifacts'). They include transients from bypassing cars ('temporal transients') or cultural noise from industrial or technical installations. These 'noise' contributions can be identified by the presented techniques. We want to emphasize the fundamental difference to the broadband 1/f seismo-acoustic background 'noise'.

• Signal (c) is a volcanic tremor signal recorded in the Fossetta on Stromboli volcano on May 24, 1994, using a Lennartz Mars-88 and a Lennartz LE-3-D sensor, natural period 1 s. The sampling rate is 62.5 Hz, file length 1 h.

• Signal (d) is a volcanic tremor signal recorded by Vilma Barboza of the Observatorio Volcanológico y Sismológico de Costa Rica at Arenal volcano, 2.8 km to the northeast of the crater on March 26, 2001, using a Kinemetrics Ranger short period seismometer model SS-1. The sampling rate is 56.6 Hz, file length 132 s.

• Signal (e) is an artificial signal consisting of a sum of sinus functions having random phases and Gaussian distributed amplitudes centered around 3 Hz:

$$e(t) = \sum_{j=-15}^{15} \exp(-j^2/30) \sin\left[2\pi(3+j/10)t + \phi\right] \quad (1)$$

where j varies in steps of 0.1, resulting in 301 terms, and ϕ is a random phase, different for each term. The amplitude of each term remains constant over time. The mean amplitude is in arbitrary units. This signal possesses all the characteristics of bandpass filtered noise, also called narrow band noise.

Fig. 4 shows a 3-s window of raw data (converted to μm/s) of the five signals. Except for signal (b), which only shows the oceanic microseism
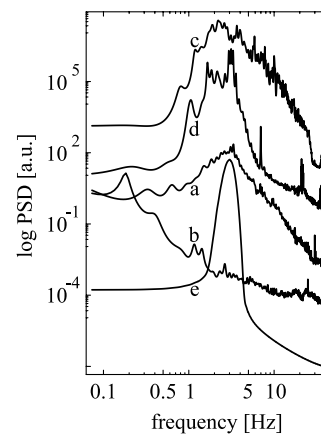

Fig. 5. Spectra of the same data as in Fig. 4. Spectra (a) and (b) are on the same scale, the other spectra have been moved vertically for demonstration reasons and are therefore not to scale.
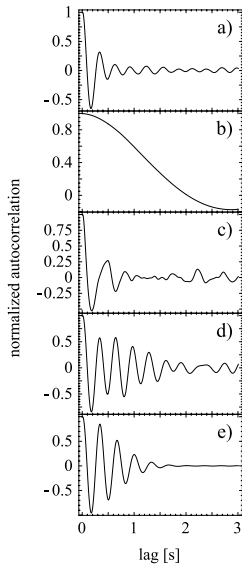
Fig. 6. Autocorrelation functions of the same data as in Fig. 4.

and some noise, the signals are quasi-periodic and look remarkably similar. Fig. 5 shows the spectra of the five signals. The maximum entropy method (Press et al., 1992) with 400 poles has been used on a time window of 500 s (132 s for Arenal). The spectra have been moved vertically in the plot for better representation and are therefore not plotted to scale. However, signals (a) and (b) are plotted on the same scale and can be compared absolutely to each other. It is interesting, although most probably not physically significant, that at least some volcanic tremor signals have their main frequencies in the same range as that of the hydrocarbon signals.

The autocorrelation functions (as one possible discriminator between stochastic and deterministic signal components) of all five signals are shown in Fig. 6. The autocorrelation function gives a measure of how long the system underlying each signal keeps memory of its past behavior, and it is used for subsequent analyses such as the embedding procedure. Typical correlation times (determined as the exponential decay rate of the envelope of the autocorrelation function) are in the 1–2-s range, with the exception of signal (b). This correlation time τ defines the width $b_p \approx 2\pi/\tau$ of the tremor peaks in the frequency

spectrum. Fortunately, τ is long enough to allow for the application of a spectral filter as follows. Because noise and especially $1/f$-noise can act on the whole chain length t_c for which the auto- or cross-correlation is performed (usually a few hundred seconds), the noise spikes in the spectrum are very narrow with half-width $b_n \approx 2\pi/t_c$, orders of magnitudes smaller than b_p of the tremor peak. By convolution of the frequency spectrum with a Gaussian $\sqrt{\pi}a \, \exp[-(\omega/2a)^2]$ satisfying $b_n \ll a \ll b_p$, the half-widths of the tremor peaks are only marginally increased but the noise spikes in the spectrum are strongly reduced. For saving computer time, the Gaussian filter is implemented in the time domain because the convolution can be transformed into a simple product there. The implementation of this filter is achieved in three steps: (1) compute the auto- or cross-correlation; (2) multiply the result with a Gaussian $\exp[-(a \, t)^2]$ (centered at the maximum correlation, at or near lag 0); and (3) Fourier transform the result in order to obtain the filtered power spectrum (the Wiener–Khinchin relationship). This filter cannot only be used to enhance the tremor signals against a noisy background, but also to increase
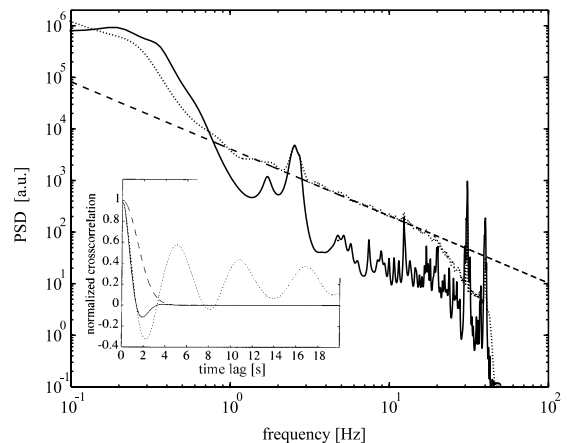

Fig. 7. An example usage of the correlation filter. The dotted line is the power spectrum obtained from one sensor, with the dashed line indicating the $1/f$ noise level of the sensor system. The solid line is the power spectrum obtained by the correlation filter as described in the text, using the crosscorrelation of two signals (horizontal distance between sensors 100 m). Inset: crosscorrelation of the two signals, Gaussian filter function (dashed line) and filtered crosscorrelation function.

the signal-to-noise level beyond the capacity of a single sensor. As an example, Fig. 7 shows raw and correlation filtered power spectra from a hydrocarbon location at site 5. The dashed line indicates the $1/f$ noise level of the sensor system. The unfiltered spectrum (dotted line) obtained from a single sensor shows the hydrocarbon tremor peak barely above the $1/f$ noise. The solid line is the spectrum obtained by cross-correlating the signal of a synchronously operating second sensor with the signal of the first sensor and using the correlation filter as described above, with $1/a = 2$ s. The horizontal distance between the two sensors was 100 m. The s/n ratio is increased by about one order of magnitude and the spectral peaks of the tremor signal become clearly visible. The narrow peaks at about 12 and 13 Hz are due to the A/C cooling system of the car used to transport the equipment, situated 300 m away from the sensors. They are not reduced by this filter because of their strong correlation and high amplitude. The inset of the figure shows the raw cross-correlation function of the two sensor signals (with the large oscillation due to the oceanic microseism), the Gaussian filter function

(dotted line) and the filtered cross-correlation, resulting from the multiplication of the raw cross-correlation function with the filter function.

A further successful tool for distinguishing time series is the structure function (Provenzale et al., 1992), used to determine self-affinity:

$$S(n) = \sum_{t=1}^{N-n} [x(t + n\,\delta t) - x(t)]^q \tag{2}$$

where N is the length of the data vector x, n the lag, δt the sampling time and $q = 2$. Fig. 8, left, shows the structure functions of the five signals. For a fractal signal, such as the z-component of the Lorenz attractor (Provenzale et al., 1992), the structure function has a scaling behavior:

$$S(n) \propto n^{2H} \tag{3}$$

for small lags n, where H is called the Hurst exponent. The Hurst exponent is a measure of the smoothness of a time series and it may be associated with the presence of long-term correlations. Hurst exponents have previously been used to characterize observed and synthetic tremors of Stromboli volcano (Urquizú and Correig, 1999). The hydrocarbon and volcanic tremor signals show the same behavior as the Lorenz attractor, including the oscillations at intermediate and constant behavior at higher lags. They all have similar Hurst exponent values around 0.9. However, the artificial signal, which by construction is not a low dimensional signal, also shows the same behavior. The structure function of signal (b) has a scaling region at higher lags only, proving its different nature. The structure functions of the first differences (derivatives) of the tremor signals shown on the right hand side of Fig. 8 reveal these differences even more effectively. Low-dimensional systems retain their scaling behavior (and correlation dimension) under differentiation, whereas stochastic systems usually do not (Provenzale et al., 1992). The structure functions of signals (d) and (e) are maintained even after differentiation. Signals (a) and (c) have a higher noise level and the structure functions of their derivatives are slightly flatter than before. However, the structure function of the derivative of signal (b) is almost flat, revealing its high dimensionality and stochastic nature. Again, all signals
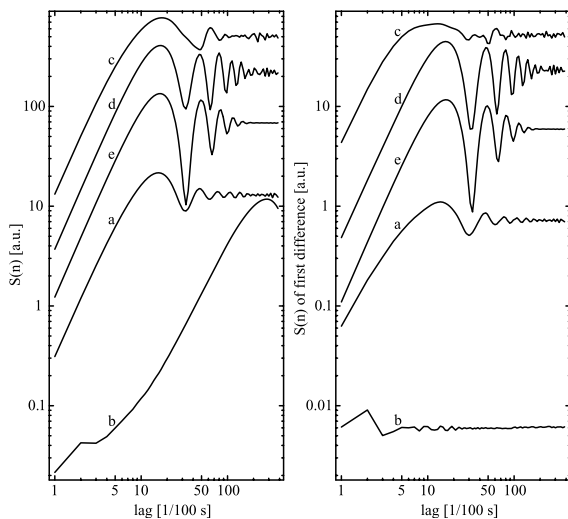

Fig. 8. Left: structure functions of the same data as in Fig. 4, moved vertically for demonstration reasons and therefore not to scale. Right: structure functions the first differences of the data, not to scale.
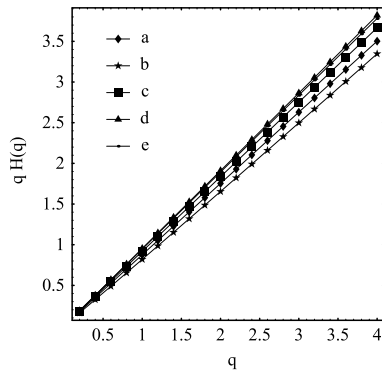
Fig. 9. The 'spectrum' of generalized Hurst exponents $q\,H(q)$ vs. q of the same data as in Fig. 4.

content and contain little or no noise, and less perfect for (a) and (c) which are spectrally broader and contain more noise. Because of the noise content or shortness – (d) is only 132 s long – of the signals, the determination of the correlation

except (b) behave similarly and cannot be significantly distinguished by this method.

Eq. 2 can be generalized to arbitrary q. The generalized Hurst exponent is then a function of q, and the 'spectrum' $q\,H(q)$ vs. q is another possible characterization of signals (Bohr et al., 1998) that can reveal the presence e.g. of a hierarchy of power law exponents. However, the 'spectra' for the five signals all grow linearly and do not have significantly different slopes as can be seen in Fig. 9. Surprisingly, this is true even for signal (b), where a completely different scaling region (at intermediate instead of small lags n) determines $H(q)$. In this case therefore the extension to the generalized Hurst exponent does not give us any further information to discriminate the signals.

In order to further characterize the signals, we performed a dimensional analysis using the standard methods of phase space reconstruction through embedding and correlation dimension estimation (Kantz and Schreiber, 1997). This may give an indication of the number of degrees of freedom of the underlying system generating the signals. As an example of phase space reconstruction we show 2-D embeddings (delay plots) of the five signals, using 600 pairs of points, in Fig. 10. As lag, the first zero of the autocorrelation functions has been used, resulting in 0.08 s for the tremor signals, equal to about one-fourth of a period, and 2 s for signal (b). The delay plot of signal (b) looks like a random walk, while the other signals result in circular figures, more perfect for (d) and (e) which have narrower spectral
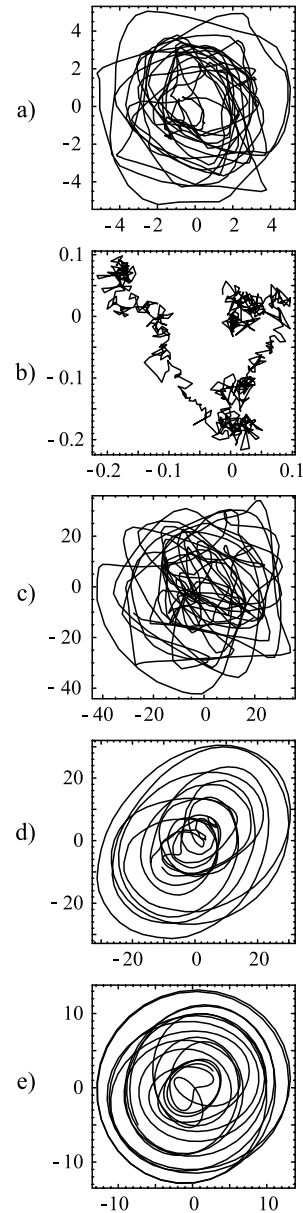

Fig. 10. 2-D delay plots of the same data as in Fig. 4, using 600 pairs of points and a delay of 0.08 s, except for signal (b), where the delay has been set to 2 s. The amplitudes are given in μm/s.
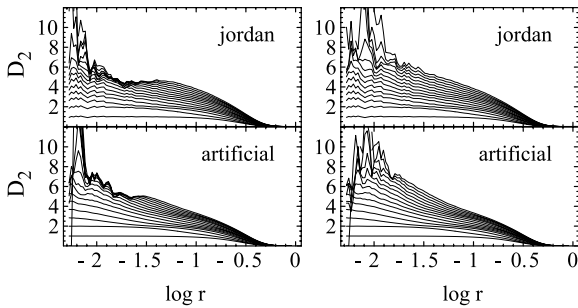
Fig. 11. Correlation dimension D_2 as a function of length scale r and embedding dimensions 1–15. 'jordan' corresponds to signal (b) of site 1, 'artificial' corresponds to the artificial tremor signal added to signal (a) of site 1. Left: using no Theiler window results in an artificially low D_2. Right: using a Theiler window of 3 s reveals the high dimensionality of the data.

dimension is difficult. Noise is high dimensional and can lead to resulting dimensions which are too high, while short time series can lead to artificially low dimensions (Kantz and Schreiber, 1997). These problems may compromise the reliability of the estimates computed on experimental data, and may explain the significantly different results found in the literature (e.g. Chouet and Shaw, 1991; Urquizú and Correig, 1999).

Nevertheless, we determined the correlation dimension D_2 of the following two signals (Fig. 11):

● 'jordan' is the raw hydrocarbon location signal of site 1, as shown in Fig. 2, which suffers from very little noise, length 20 000 data points.

● 'artificial' is the artificial signal (e) as defined above, added to the raw non-hydrocarbon location signal of site 1, as shown in Fig. 2, with amplitudes at approximately the same proportions as the two spectral peaks of the 'jordan' signal, length 20 000 data points.

We believe that it is safer to compare the so constructed artificial signal to the original hydrocarbon location signal than to filter the latter in order to remove the oceanic microseism and some of its noise (for the definition of which a criterion would have to be defined first: the percentage of non-deterministic dynamics can e.g. be determined with the method of false nearest neighbors (Carniel and DiCecca, 1999; Kantz and Schreiber, 1997)), both of which are not contained in signal (e). The program 'd2' contained in the TI-

SEAN package (Hegger et al., 1999) has been used to determine the correlation sums. For the plots on the left hand side of Fig. 11, no care is taken to exclude time correlated points in the calculations. The plots suggest a dimension of about 4–5 for both signals. However, the saturation of D_2 as a function of the embedding dimension is suspiciously slow. When temporally correlated points of the attractor (i.e. the ones belonging to the so-called Theiler window; see Kantz and Schreiber, 1997) are excluded in the correlation sums by the application of a Theiler window (right hand side of Fig. 11), no saturation of D_2 as a function of the embedding dimension can be found at all. Thus we may conclude that the time correlation of the signals leads to an artificially low value for D_2 when no care is taken to exclude time correlated points. It has been shown before that narrow band noise, although high dimensional, can mimic chaotic behavior (Rapp et al., 1993).

Even though we cannot report the finding of low dimensionality in our data (in contrast to e.g. Chouet and Shaw, 1991, reporting correlation dimensions of about 4 for tremor signals of Kilauea volcano), we suggest that the correlation dimension may still be used as a relative indicator for dimensionality, which can still be practical to distinguish signals containing tremor from signals which do not. The results should not be interpreted as absolute values of dimension, following an interpretation as taken e.g. by Widman et al. (2000) for electroencephalogram time series.

As a last tool used to distinguish time series, we have calculated bispectra and bicoherences (Rao and Gabr, 1984) of our signals. Fig. 12 shows the results for signals (a) and (c). The results for the other signals, again with the exception of (b), which only shows features below 1 Hz which can be attributed to the oceanic microseism, are analogous and have been omitted to save space. As the power spectrum of a real time series can be seen as the Fourier transform of its autocorrelation function or second-order cumulant $\langle x(n) x(n+k)\rangle$, the bispectrum is the 2-D Fourier transform of its third-order cumulant $\langle x(n) x(n+k) x(n+l)\rangle$. It is a function of two frequencies and has the property to be non-zero if the data are
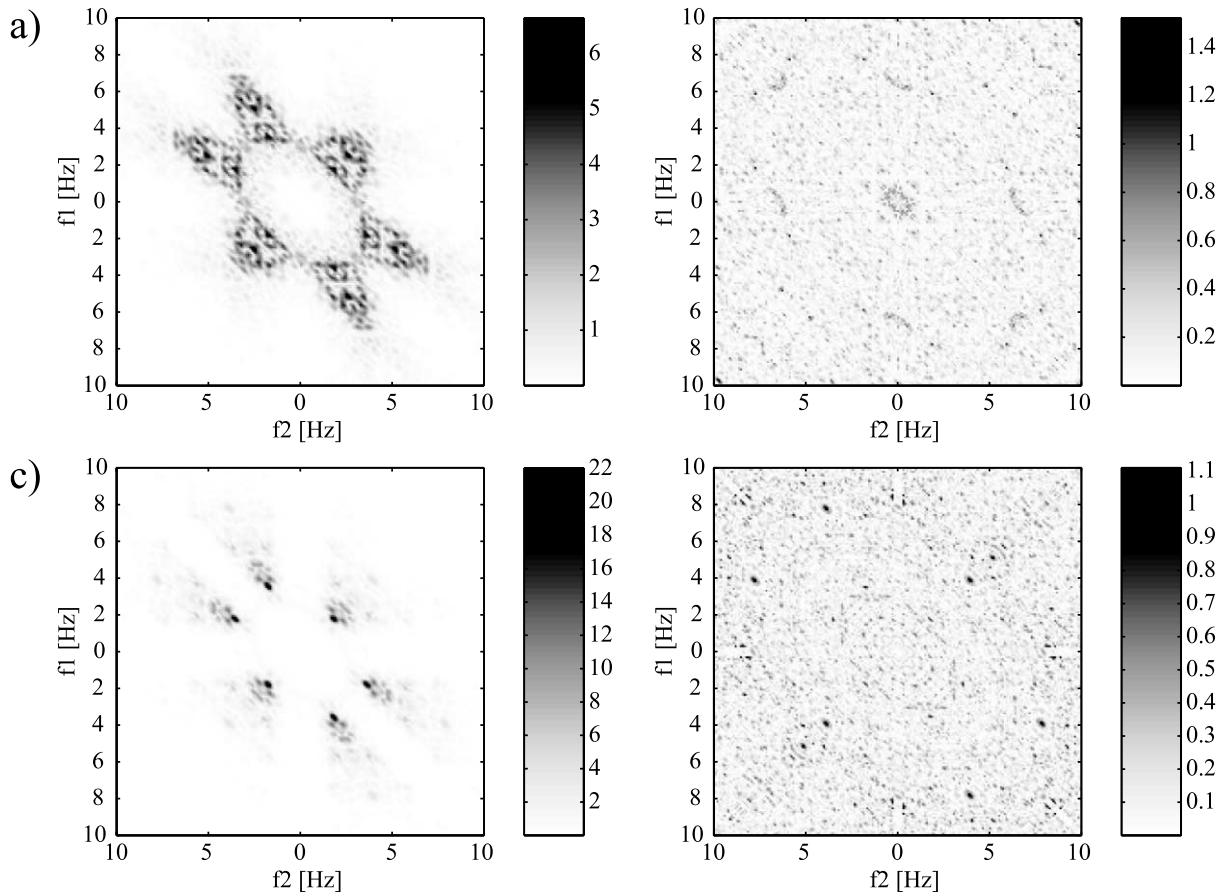
Fig. 12. Bispectra (left) and bicoherences (right) of data (a) and (c) as in Fig. 4.

non-Gaussian (the inverse is not necessarily true). The bicoherence is the bispectrum weighted by the spectrum of the signal; see Rao and Gabr, (1984) for a more precise definition. If the bispectrum is non-zero and the bicoherence is constant, then the underlying process is non-Gaussian and linear. Fig. 12 shows non-zero bispectra and non-constant bicoherences for both signals. We therefore conclude that the tremor data are non-Gaussian and (at least to a certain extent) non-linear.

From the results of the different data comparison methods of this section, we conclude as already indicated above, that we find significant evidence that the recorded tremor signals may be interpreted as narrow band ('filtered') noise (with certain implications for their microscopic origin, see below).

4. Tremor and practical hydrocarbon detection

In this section we discuss the recorded hydrocarbon tremor signal with respect to its relevance for hydrocarbon detection. ADNR uses a commercialized setup called ADNR Explorer. We show and discuss the results of one of the campaigns carried out in the UAE, site 5 of the above reference site list, here called Q-field. This field has been explored and proven via exploration wells. The main production zone is a carbonate reservoir called Thamama. Since the field is not yet developed or in production, the area is very quiet and therefore ideal for tremor measurements. We have carried out two data acquisition campaigns with a time lag of several months in between (May and November 2000), and at most
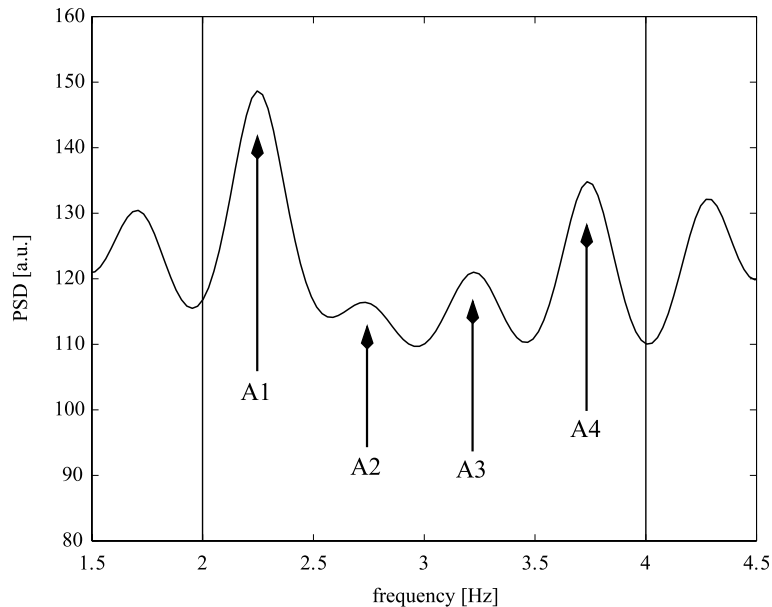
Fig. 13. Power spectrum corresponding to well Qw-5 of site 5. The four spectral peaks in the frequency window 2–4 Hz are characteristic of the hydrocarbon locations of this site.

measurement points data have been recorded several times even within a single campaign. Both types of sensors have been used in different combinations.

Fig. 13 shows a typical spectrum (from a time window without artefacts) recorded close to one of the exploration wells, Qw-5, and showing the spectral window of interest. Clearly there are four spectral peaks (lines) visible in the frequency window 2–4 Hz, denoted as lines A1, A2, A3 and A4. These four lines are characteristic of all oil-bearing locations of this field, with a small scatter in their respective frequency location and different absolute and relative amplitudes. Those four lines are used to construct a quantitative indicator giving the 'hydrocarbon tremor power'. As will be shown below, it turns out to be a rather nice direct hydrocarbon indicator.

The tremor power is constructed as:

$$A1234 = (A1 + A2 + A3 + A4)/4, \ k = AN1/AN5$$

with Ai being the absolute amplitude at the spectral line Ai, and $AN1$, $AN5$ being the amplitude level below and above the investigated window at frequencies 1 Hz and 5 Hz. The factor k gives the

slope of the spectrum towards higher frequencies, and works as a 'zero-order' correction of external higher frequency influences. The final indicator ('normalized corrected tremor power') is then calculated as:

$$kA1234 = kA1234/\max(A1234)$$

with $\max(A1234)$ being the maximum of the averaged amplitudes in the investigated area or profile.

The evolution of the recorded spectrum along a NE–SW profile crossing several oil-bearing compartments in Q-field is illustrated on the map of the area in Fig. 14. One can clearly see that the spectra undergo an evolution when oil-bearing zones, non-oil zones, oil–water contacts and other structural elements within the reservoir zone (such as faults) are crossed. The corresponding Fig. 15 gives a plot of the hydrocarbon tremor power $kA1234$ along this very same profile. The locations of existing exploration wells are indicated by arrows. There is an additional interesting fact to note: the tremor power is very small at well Qw-4, which is actually touching the oil–water contact and is producing water only (20 barrels
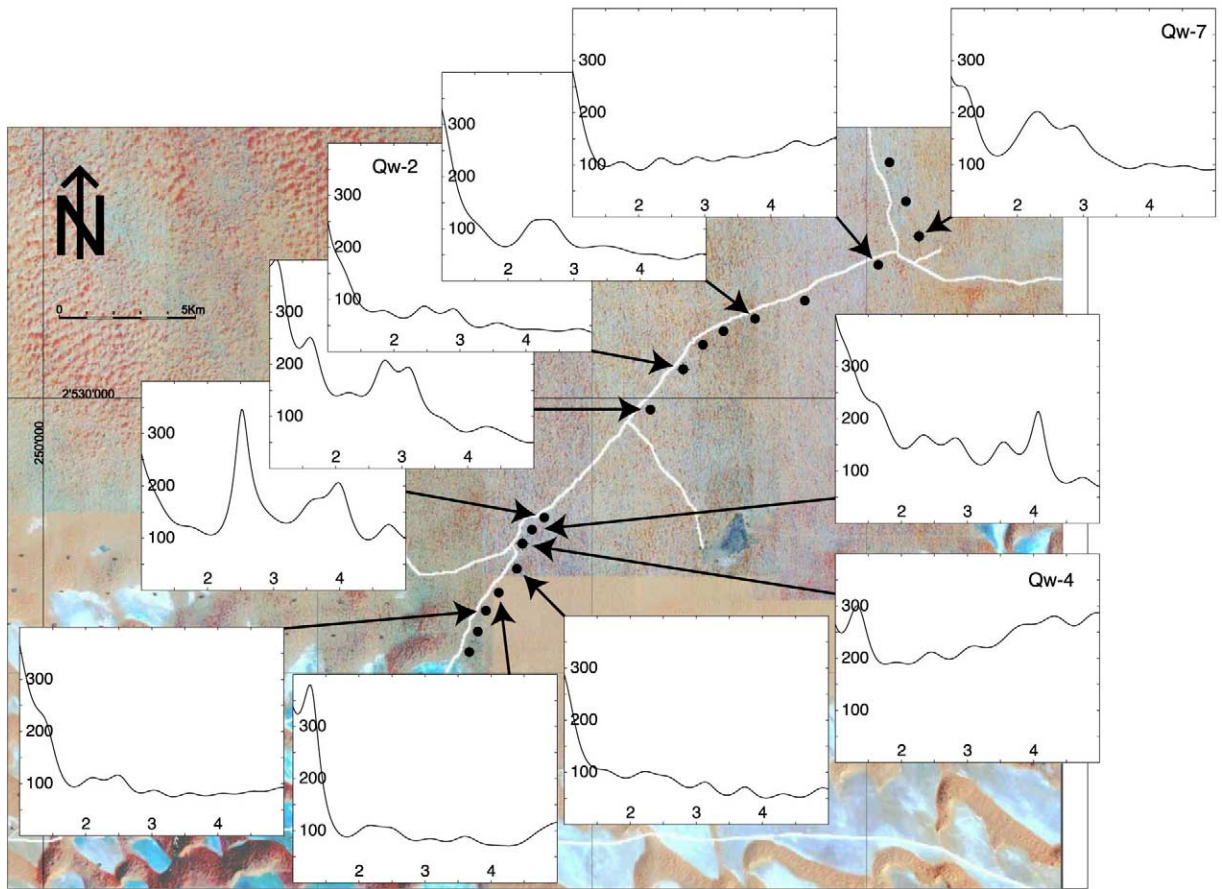
Fig. 14. Map of site 5, 'Empty Quarter', UAE. Only the measurement points along a NE–SW profile (given by the sand road depicted as a bright line in the map) and some of the corresponding spectra (horizontal units Hz, vertical units a.u.) are shown. The locations designated Qw-n correspond to well locations. The background map gives a satellite picture of the surface topography, with medium high (up to 20 m) dunes in the area of the recorded profile and ultra high (up to 300 m) dunes in the area to the south.

of water per day as a testing result). Just after Qw-4 along the profile there is a very high reading of the tremor power. This indicates a structural compartment and a fault zone running between Qw-4 and the next measuring point (at 14.5 km). Interestingly enough this finding is confirmed by a reflection seismic campaign carried out some time before, which clearly indicates a fault running perpendicularly to the profile at this point, but, of course, gives no hint on the actual hydrocarbon distribution. Additionally, the operator of the particular field has successfully crosschecked our results with his proprietary reservoir model for this particular field (derived from
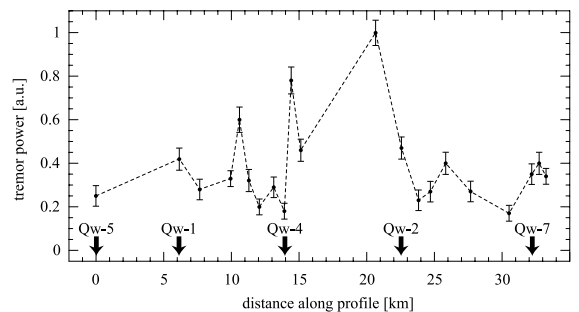

Fig. 15. 'Hydrocarbon tremor power' along the same NE–SW profile as in Fig. 14, site 5. The locations of existing exploration wells are indicated by the arrows and their names Qw-n.
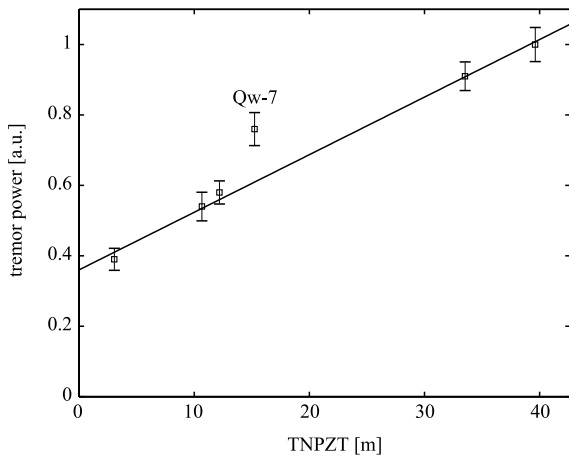
Fig. 16. Correlation of observed hydrocarbon tremor power with the total net pay zone thickness (TNPZT) at the exploration wells along the NE–SW profile of site 5. Only well Qw-7 lies off an almost perfect linear correlation. The suspected explanation is that Qw-7 is located over a deeper reservoir zone which is not penetrated by the borehole and thus the log does not account for the additional pay zone. There is considerable evidence for this deeper Jurassic zone.

seismic and exploration well logging and testing data).[3]

Finally, Fig. 16 tries to correlate our readings of the hydrocarbon tremor power as observed on the surface with known reservoir parameters. The tremor power $kA1234$ is plotted against the so-called total net pay zone thickness ('TNPZT') of the reservoir. The pay zone is the actual oil-bearing zone, its net thickness, as it is determined by borehole logs, is the overall thickness of the multiple reservoir (hydrocarbon-bearing) stacks (in short, the total thickness of the hydrocarbon-bearing reservoir layers). As can be seen in Fig. 16, the correlation is very good, with only well Qw-7 slightly off a perfect correlation. Qw-7 has only been drilled down to its intended target depth in the reservoir zone Thamama-F, accounting for a total of approximately 15 m of pay zone thickness. The tremor power reading is much higher, corresponding to a 'virtual' total pay zone thickness of about 25 m. The missing 10 m

of pay zone are believed to be found in a deeper Jurassic reservoir zone, for which clear indications from reflection seismics exist. This deep lying reservoir zone has a 'finger' reaching below well Qw-7 in the Q-field, with well Qw-7 being located at the very end of the profile. Therefore, the correlation between surface spectroscopic measurements and subsurface reservoir properties is indeed existing and confirmed. It should be noted that the six values of the tremor power in Fig. 16 have been calculated separately, using a normalization with the maximum resulting from just the six well data sets. Thus, the dynamic range for this plot is again [0;1], but the numbers do not directly compare to the previous figure. The error bars drawn on the data points (typically of an average order of ±2–5%) in Fig. 15 and 16 have been calculated using the statistics of long records (windowing of long records into shorter pieces, statistics over those pieces) as well as repeat measurements within the same campaign and at the second campaign carried out at the same location five months later. They are purely statistical quantities. The internal equipment measurement uncertainties (recorder, etc.) are orders of magnitude smaller and, thus, simply neglected.

We did not succeed in establishing a correlation with any other characteristic reservoir property so far. The tested parameters include the absolute depth, pressure, temperature, etc. as well as more dynamic quantities like production rate, permeability, and depth. The tremor power (amplitudes of the characteristic lines) does not depend on depth changes. Phenomenologically, it is reasonable that a process generating the particular spectroscopic characteristics in the seismic background signal does depend on the thickness of the reservoir layer, independent whether we assume an active signal generation in the reservoir or a passive signal filtering through the reservoir. Particularly, if the reservoir works as a filter for the seismic background noise, it is quite obvious that the signal amplitude measured at the surface has a direct relation to the filter strength, and in turn the filter strength is connected to the filter thickness, assuming that the filter properties are equal over the reservoir cross section.

These correlation studies have been successfully

---

[3] Unfortunately, we are not allowed to publish the detailed model.

verified at other locations where a sufficient number of existing boreholes and, thus, subsurface data exist. We want to remark on two quite interesting results: Site 4 (see Section 3.1) is a heavily producing field, and some of the wells have been continuously producing at quite high rates for more than 20 years. The data provided from the operator were so-called 'original' well logs acquired at the time when the well had been drilled. When we established a similar correlation plot (correlation coefficient 0.90) for the approximately 20 wells located in this area, we found three pathological cases. A thorough investigation found out that all three wells had serious engineering problems, such as casing failures and water break-in into the reservoir or water-coning, effectively reducing the thickness of the reservoir zone of those three wells significantly. The estimates produced by the surface spectroscopy measurements are believed to reflect the current reservoir zone much more realistically. Site 13, as indicated before, is a quite interesting system, too, as it consists of one oil-bearing subsurface structure (anticline), which is effectively divided into two disconnected reservoirs by a tight permeability barrier crossing the reservoir. From both parts of the reservoir there is a production of gas and gas condensate, but only into one reservoir part dry gas is reinjected for storage purposes (the operator is currently interested mostly in the condensate fraction). As a consequence the correlation plot splits up into two distinct branches, with all the wells in the production-only part falling onto one sharp line, whereas all the other wells from the production and reinjection part of the field drop onto another, very distinct line. We interpret this effect as two distinct physical systems in front of a common 'background illumination'. The different fit curves would effectively reflect the distinct parameters for the two different physical systems. As a side note we would like to emphasize that a quantitative comparison of the absolute spectroscopic data produced at different locations worldwide is only possible if the complete spectroscopic process is under control. As we believe that the presented process is driven by the overall amplitude of the seismo-acoustic background, it is necessary to control this ampli-

tude. The seismo-acoustic background is believed to be a stochastic, $1/f$ background, and this very characteristic can be used to identify the background amplitude nicely via the zero-time-lag autocorrelation amplitude. Studies on this topic are subject of our current research activities.

Moreover, it should be noted that we do not find an obvious relation between the particular frequency of the hydrocarbon tremor lines and a series of reservoir parameters tested, including pay zone thickness, depth and pressure. Possible correlations of the tremor peak widths and reservoir parameters are a matter of future investigations.

More 'conventional' explanations of low-frequency spectral signatures in a hydrocarbon reservoir would include the possible appearance of tube waves at wells/bore holes. We do exclude such an effect because of the following series of observations which we think are not congruent with tube wave excitations.

● Tube waves would only appear in a developed field where bore holes exist. We explored one hydrocarbon prospect where no holes had been drilled within a distance of approximately 100 km at the time of signal recording.

● Tube waves at wells may be either of the 'pipe oscillation' type, i.e. a geometric excitation of the bore hole cylinder and casing, or of the fluid oscillation type, i.e. the fluid penetrating through the perforated casing may oscillate. Both types are highly improbable due to the fact that: (a) such an oscillation is strongly geometry dependent, and the particular frequency spectrum would vary from well to well, in contrast to our observations; (b) the amplitude of such oscillations does drop off very rapidly and characteristically as a function of distance receiver–borehole, which is not observed at all in any of the measurements performed; and (c) this kind of tube resonances would create a very well defined resonance spectrum with a basic frequency and easily identifiable higher multiples, the frequency distribution of them would depend on the tube geometry. Again, nothing like this is observed.

Of these arguments, the 'universality' of the hydrocarbon spectral signature through a large series of hydrocarbon reservoirs all over the world

contradicts such a more conventional explanation of distinct spectral features.

5. Discussion

In this section, we point to some additional findings which give certain hints about the origins of hydrocarbon tremor.

In areas with medium to high seismo-acoustic noise level, the hydrocarbon tremor signal has been observed to be (quasi) continuous. In Fig. 17, the spectrograms of the hydrocarbon location signal of site 9 (as in Fig. 2) and of the volcanic tremor signal from Stromboli are compared. These two signals correspond to the signals dubbed (a) and (c) above. The time resolution is 10 s, and 1 h of each signal is shown.

In order to see if the hydrocarbon tremor depends on a controlled external seismic input signal, tests using vibrators on the surface have been made at sites 2 and 3. Standard vibrators as used for seismic campaigns have been employed in frequency sweep (8–15 Hz) and single frequency modes. When comparing the tremor signals be-

fore, during and after vibration, no consistent change could be observed. However, this could also be due to the fact that, compared to the seismo-acoustic noise, very little energy of the vibrators reaches the actual reservoirs to stimulate the observed effect. This, of course, is a conclusion based on the following facts: (a) the natural seismo-acoustic background has a $1/f$-behavior in the frequency window of interest, giving a strongly increasing amplitude towards lower frequencies; and (b) in comparison with the natural seismo-acoustic background artificial sources such as vibroseis devices tend to be extremely weak towards low frequencies; explosive sources with a more broadband signature are too difficult to control in the required *amplitude* range (i.e. relative to the natural background). This does not at all contradict the successful application of artificial sources in conventional refraction seismic processes, as those deal with a completely different physical process, namely the detection of a controlled input signal after one or several refractions/reflections. The stimulation of the observed hydrocarbon tremor is a totally different physical effect.
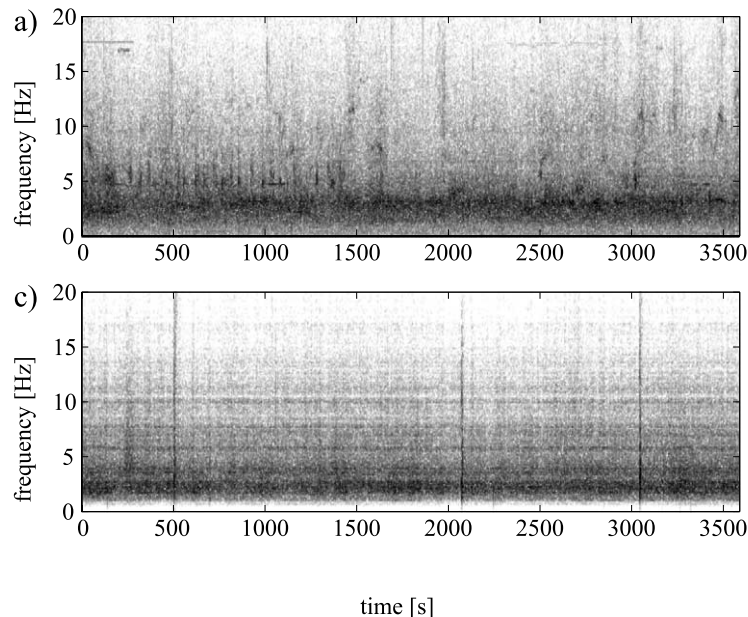

Fig. 17. Spectrograms of the hydrocarbon signal (a) and volcanic signal (c) as in Fig. 4, 1 h time window, 10 s time resolution.

However, in areas with a low seismo-acoustic noise level, the hydrocarbon tremor signal can show significant time variations. As an example, Fig. 18 shows the wavelet analysis of an 'event' that occurred at a hydrocarbon location of site 4. Wavelets (Mallat, 1999) can be used to decompose a signal into individual frequency components at much higher time resolution than spectrograms. For our purposes, the wavelet kind called 'Morlet' has proven to be ideal. Fig. 18 shows the coefficients of the Morlet decomposition of the signal as a function of time for three different wavelet scales, which are inversely proportional to the frequency content. An event with unknown origin (no vibrator or explosion has been used, the environment at the surface was quiet at this time) occurs at $t \approx 55$ s, as can be seen in all three frequency bands. Shortly after this time, the two frequency bands around 1 and 6 Hz return to their normal (noise) amplitude level, while the 3-Hz band shows an oscillatory behavior. It seems to be amplitude modulated with a time period between maxima of about 14 s and decays more or less exponentially within about 40 s. This behavior has been observed at several hydrocarbon locations of sites 4 and 5. Its origin remains a puzzle, as does the modulation time, which is too long for reflections of the signal between the reservoir and the surface (the ratio of the depth to the speed in the overlying rocks is about one second). There exists a very slow type of wave inside the reservoir, the so-called Biot slow wave (Biot, 1956). However, it is very strongly damped and therefore no reflections within the reservoir boundaries of such waves are expected to occur.

Fig. 19 gives another hint for the source of hydrocarbon tremor. At site 7, one of the producing gas wells was closed or under repairs in November 1999. The figure shows amplitude spectra of the hydrocarbon tremors observed in May 1999, before the shutdown (bottom left), and in February 2000, after the shutdown (bottom right). The narrow peak at about 1.4 Hz is a man-made artifact originating from a pump. In the second measurement, the amplitude of the tremor has increased by about one order of magnitude. At the measurement points situated around this gas
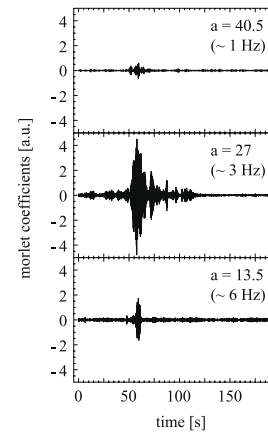

Fig. 18. An event of unknown origin seemingly triggering the source of the hydrocarbon tremor at a hydrocarbon location of site 4. Using a wavelet decomposition of the signal, the event starting at $t \approx 55$ s can initially be seen in all three frequency bands, afterwards only in the hydrocarbon tremor frequency band at around 3 Hz. The remaining signal seems to be amplitude modulated and to decay exponentially. The time period between the maxima is approximately 14 s. The coefficient a is the scale of the corresponding Morlet wavelet and is inversely proportional to its frequency content.

well, the tremor amplitudes obtained by the two measurements were equal within 10%. A separate third campaign confirmed these findings. One of the known changes occurring when a well is closed is an increase in fluid pressure around the well. When hydrocarbon production from a well is going on over a long period of time, it is known that a pronounced bottom hole pressure reduction develops. As a consequence a reduction in the hydrocarbon column in the vicinity of the wellbore will be established due to either free gas moving down or water moving up in the well area of the oil reservoir (see Fig. 19, top). This reduction of the hydrocarbon column associated with production tends to vanish and the system tries to return to the original state when the well is shut in and the pressure builds up again due to the flow of hydrocarbons from distant parts of the reservoir (Dake, 2001). Since we have not observed any correlation of the hydrocarbon tremor amplitudes with reservoir depth, to which the pressure is more or less proportional, but a very good correlation with the total net pay zone thickness, we believe that the increased fluid sat-
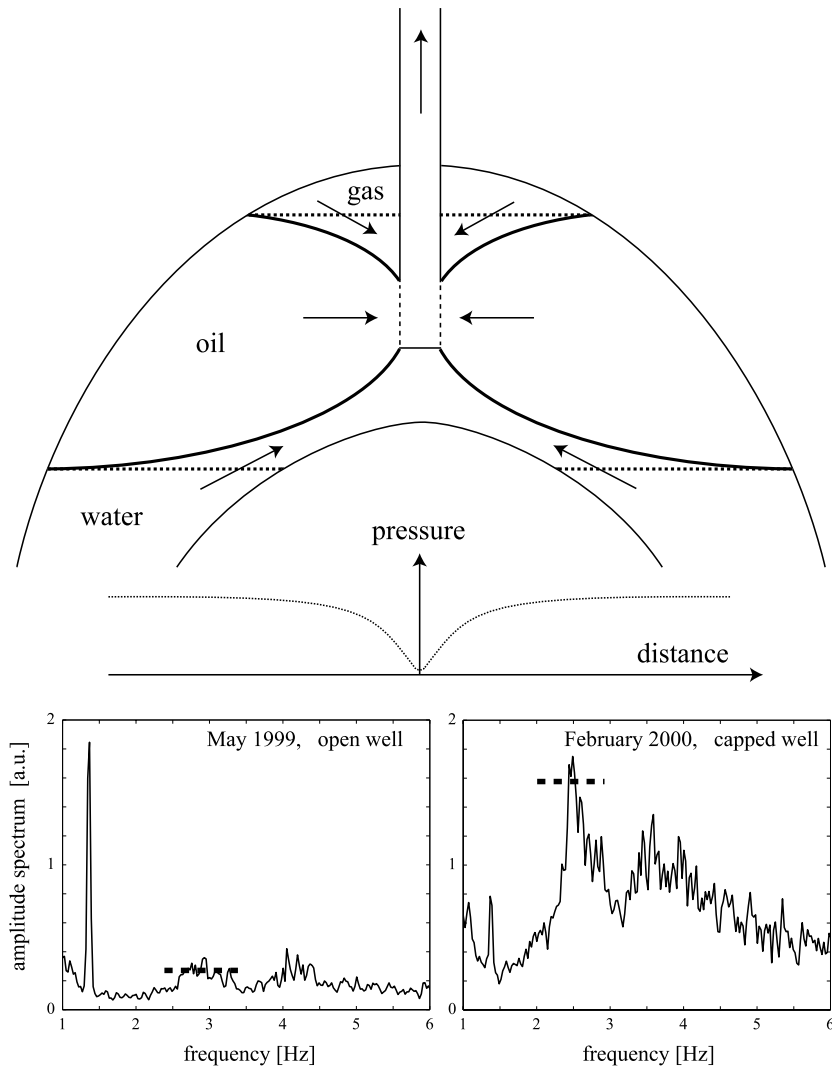
Fig. 19. Comparison of spectra obtained at the same gas well location of site 7 at two different measurement campaigns. The well was open when measurement 1 (bottom left) was made in May 1999, closed in November 1999, and still closed when measurement 2 (bottom right) was made in February 2000. At the measurement points situated around this well, no such discrepancy could be observed. The narrow peak at about 1.4 Hz is a man-made artifact originating from a pump. The schematic drawing shows the disturbance of the gas, oil and water layers due to an operating well and the resulting pressure disequilibrium, see text.

uration is responsible for this remarkable increase in hydrocarbon tremor amplitude.

At this stage, we believe that the main effect leading to our observation of hydrocarbon tremor is a source, rather than a path effect (Correig and Vila, 1993). This is due to the fact that the signals have very similar characteristics at all surveyed sites, while the overlying geology and the depths

are quite different from site to site. The source models proposed so far for volcanic and glacial tremor, e.g. hydraulic transients (Lawrence and Qamar, 1979), non-linear fluid flow (Julian, 1994), and gas bubbles (Ripepe and Gordeev, 1999; Ripepe et al., 2002), result in spectral peaks located at frequencies that are influenced by the geometry of the fluid-filled conduits (Ferrazini

and Aki, 1987). Slow fluid flow is very well possible in (even non-producing) hydrocarbon reservoirs. The driving mechanisms are gravity and pressure differences due to natural causes or due to non-steady production. However, our results suggest that the source mechanism for the hydrocarbon tremor must be independent of the pore geometry of the reservoir rocks (Radlinski et al., 1999) or the geometry of fractures in the reservoir, since the observed spectral peaks lie within a very small frequency range for all reservoirs surveyed up to this time. Fluid induced seismicity at relatively high frequencies is a well-known phenomenon in porous reservoirs (Shapiro et al., 1999), but the received signals are short cracking events. However, fluid flow is not the only possible source for hydrocarbon tremor. Surface tension between, for example, oil and water can lead to oscillations of boundary surfaces (Dimon et al., 1988) confined by the pore geometry (Hilpert et al., 2000), perhaps driven by the energy of some of the low-frequency seismic background noise. Of course, a synchronization mechanism would be necessary in order to make the signals of a large number of those single oscillators observable. This would split the basic mechanism into two parts, a microscopic oscillation/resonance and a macroscopic synchronization of the numerous single pore 'resonances' via e.g. a low-frequency component of the background ('synchronizing external wave field'). Since the size of the oil surface increases with the thickness of the pay zone (assuming an otherwise homogeneous reservoir), a possible surface tension effect would agree well with the excellent correlation shown in Fig. 16. However, in such a mechanism a geometry dependent contribution might still be involved. Unfortunately, the fact that our tremor data seem to be equivalent to filtered noise does not discriminate between these macroscopic (fluid flow) or microscopic (surface effects) views. Filtered noise can be, as the name suggests, the result of filtering noise, or the result of a superposition of many oscillations, as we constructed our artificial data above, or even transients. This last model would be somehow similar to the one proposed by Ripepe and Gordeev (1999) for volcanic tremor. As in that case, the final spectrum may be strongly influenced by the comb effect given by the superposition of the single signals.

In the proper filtered noise model, the reservoir would act not directly as a source of tremor, but as a bandpass filter acting on the seismic background noise and amplifying the observed peak frequencies. The fact that the absolute power of the hydrocarbon tremors depends on the level of the environmental noise might speak for such a filter effect. A similar phenomenon is well known in earthquake engineering, leading to site amplification of earthquake damages that can be investigated using, for example, Nakamura's spectral ratio method (Nakamura, 1989). However, a preliminary analysis of some three component recordings shows a trough instead of a peak in the horizontal to vertical ('H/V') ratio in the hydrocarbon tremor frequency band. On one hand, this fact might speak against site amplification; on the other hand, it could be explained by a different interpretation of the H/V spectral ratio method, which is commonly used but still rather poorly theoretically understood (Bard, 1999). In any case, it will be a subject of future research.

6. Conclusions

In conclusion, we have observed characteristic narrow-band tremor signals ('hydrocarbon tremor') over a large series of hydrocarbon reservoir sites. Even though the geological properties, the reservoir types and the specific characteristics of the seismo-acoustic background noise ('spectroscopic illumination') differ widely, the observed signals possess remarkably similar characteristics, particularly similar spectroscopic signatures, in the low-frequency window investigated. This suggests a common source or filtering mechanism inside the reservoir zone and excludes e.g. a simple path effect.

Phenomenologically, we find a kind of signal which appears to be very similar to known tremor phenomena originating at volcanoes, as described above. The so-far applied methods resemble qualitatively the methods applied in volcanology. Nevertheless, it is obvious that the specific signal sources are expected to be different for volcanoes

and hydrocarbon reservoirs despite an astonishing similarity of the hydrocarbon tremor in terms of signal type, properties and structure to the volcanic tremor.

The strong relation between hydrocarbon tremor properties and reservoir parameters such as the pay zone thickness gives clear evidence that: (a) the signal results from an effect in the reservoir itself, and (b) the described phenomenon is an excellent from-the-surface hydrocarbon reservoir prospection method (direct hydrocarbon detector). The presented results and arguments give strong evidence that we are observing an effective filtering/mixing effect in the reservoir. The ambient seismo-acoustic background noise, present everywhere on earth with varying overall amplitude, is the 'initial supply' of a broadband input for this filtering/mixing process. The hydrocarbon reservoir merely leaves a spectroscopically detectable fingerprint in this background signal.

The so-far presented results provide only a 2-D view, thus, giving only information about 'net' quantities, such as the net pay zone thickness. In stacked multi-horizon reservoir systems a depth resolution (depth triangulation, 3-D measurement) is required. We therefore plan to acquire new hydrocarbon tremor data focusing on the use of 3-component seismometers, and direction-sensitive sensor arrays ('seismic antennas'), which can be constructed according to the very same design criteria as applied in volcanology research (Wassermann, 1997; Saccorotti et al., 2001). Since the wavelength of the tremor signal inside the overlying rocks is comparable to the depth of the reservoirs, near field effects will have to be taken into account (Stoll and Dangel, 2001), and they are expected to be significant.

References

Aki, K., Richards, P.G., 1980. Quantitative Seismology: Theory and Methods. Freeman.

Bard, P.-Y., 1999. Microtremor measurements: A tool for site effect estimation? In: The Effects of Surface Geology on Seismic Motion. Bakema, Rotterdam, pp. 1251–1279.

Biot, M., 1956. Theory of propagation of elastic waves in a fluid-saturated porous solid, I. Low-frequency range. J. Acoust. Soc. Am. 28, 168–178.

Bohr, T., Jensen, M.H., Paladin, G., Vulpiani, A., 1998. Dynamical Systems Approach to Turbulence. Cambridge University Press.

Carniel, R., DiCecca, M., 1999. Dynamical tools for the analysis of long term evolution of volcanic tremor at Stromboli. Ann. Geofis. 42, 483–495.

Carniel, R., Iacop, F., 1996. Spectral precursors of paroxysmal phases at Stromboli. Ann. Geofis. 39, 327–345.

Chouet, B., Shaw, H.R., 1991. Fractal properties of tremor and gas piston events observed at Kilauea Volcano, Hawaii. J. Geophys. Res. 96, 10177–10189.

Correig, A.M., Vila, J., 1993. On the frequency contents of local events: Source or path effect? Geophys. J. Int. 115, 863–877.

Dake, L.P., 2001. The Practice of Reservoir Engineering. Elsevier, Amsterdam.

Dangel, S., Singer, J.M., 2002. Observation of characteristic tremor phenomena over hydrocarbon reservoirs (to be submitted).

Dimon, P., Kushnick, A., Stokes, J., 1988. Resonance of a liquid–liquid interface. J. Phys. Fr. 49, 777–785.

Ferrazini, V., Aki, K., 1987. Slow waves trapped in a fluid-filled infinite crack: Implications for volcanic tremor. J. of Geophys. Res. 92, 9215–9223.

Ferrick, M.G., Qamar, A., Lawrence, W.F.S., 1982. Source mechanism of volcanic tremor. J. Geophys. Res. 87, 8675–8683.

Hegger, R., Kantz, H., Schreiber, T., 1999. Practical implementation of nonlinear time series methods: The TISEAN package. Chaos 9, 413–435.

Hilpert, M., Jirka, G., Plate, E., 2000. Capillarity-induced resonance of oil blobs in capillary tubes and porous media. Geophysics 65, 874–883.

Julian, B.R., 1994. Volcanic tremor: Nonlinear excitation by fluid flow. J. Geophys. Res. 99, 11859–11877.

Kantz, H., Schreiber, T., 1997. Nonlinear Time Series Analysis. Cambridge University Press.

Lawrence, W.S., Qamar, A., 1979. Hydraulic transients: A seismic source in volcanoes and glaciers. Science 203, 654–656.

Mallat, S., 1999. A Wavelet Tour of Signal Processing, 2nd ed. Academic Press, London.

Nakamura, Y., 1989. A method for dynamic characteristics estimation of subsurface using microtremor on the ground surface. Quarterly Report of the Railway Technical Research Institute 30.

Press, W.H., Teukolsky, S.A., Vetterling, W.T., Flannery, B.P., 1992. Numerical Recipes in Fortran, 2nd ed. Cambridge University Press.

Provenzale, A., Smith, L., Vio, R., Murante, G., 1992. Distinguishing between low-dimensional dynamics and randomness in measured time series. Physica D 58, 31–39.

Radlinski, A., Radlinska, E., Agamalian, M., Wignall, G., Lindner, P., Randl, O., 1999. Fractal geometry of rocks. Phys. Rev. Lett. 82, 3078–3081.

Rao, T.S., Gabr, M.M., 1984. An Introduction to Bispectral Analysis and Bilinear Time Series Models. Springer.

Rapp, P., Albano, A., Schmah, T., Farwell, L., 1993. Filtered noise can mimic low-dimensional chaotic attractors. Phys. Rev. E 47, 2289–2297.

Ripepe, M., Gordeev, E., 1999. Gas bubble dynamics model for shallow volcanic tremor at Stromboli. J. Geophys. Res. 104, 10639–10654.

Ripepe, M., Harris, A.J.L., Carniel, R., 2002. Thermal, seismic and infrasonic evidences of variable degassing rates at Stromboli volcano. J. Volcanol. Geotherm. Res. 118, 285–297.

Saccorotti, G., Maresca, R., DelPezzo, E., 2001. Array analyses of seismic noise at Mt. Vesuvius volcano, Italy. J. Volcanol. Geotherm. Res. 110, 79–100.

Shapiro, S.A., Audigane, P., Royer, J.-J., 1999. Large-scale in situ permeability tensor of rocks from induced microseismicity. Geophys. J. Int. 137, 207–213.

Stoll, E.P., Dangel, S., 2001. Numerical solution of the acoustic wave equation at the limit between near and far field propagation. Int. J. Mod. Phys. C 12, 1497–1508.

Suda, N., Nawa, K., Fukao, Y., 1998. Earth's background free oscillations. Science 279, 2089–2091.

Urquizú, M., Correig, A.M., 1999. On the spectral peaks of volcanic tremor at Stromboli. Phys. Earth Planet. Inter. 110, 247–261.

Wassermann, J., 1997. Locating the sources of volcanic explosions and volcanic tremor at Stromboli volcano (Italy) using beam-forming on diffraction hyperboloids. Phys. Earth Planet. Inter. 104, 271–281.

Widman, G., Schreiber, T., Rehberg, B., Hoeft, A., Elger, C.E., 2000. Quantification of depth of anesthesia by nonlinear time series analysis of brain electrical activity. Phys. Rev. E 62, 4898–4903.

Wolf, L.W., Davies, J.N., 1986. Glacier-generated earthquakes from Prince William Sound, Alaska. Bull. Seismol. Soc. Am. 76, 367–379.